Cell Host & Microbe
Article

Cholera Toxin Disrupts Barrier Function by Inhibiting Exocyst-Mediated Trafficking of Host Proteins to Intestinal Cell Junctions

Annabel Guichard,[1] Beatriz Cruz Cruz-Moreno,[1] Berenice Aguilar,[2] Nina M. van Sorge,[2,6] Jennifer Kuang,[1] Adrianne A. Kurkciyan,[1] Zhipeng Wang,[5] Saiyu Hang,[5] Guillaume P. Pineton de Chambrun,[3] Declan F. McCole,[3,7] Paula Watnick,[5] Victor Nizet,[2,4] and Ethan Bier[1,*]
[1]Section of Cell and Developmental Biology
[2]Department of Pediatrics
[3]Department of Medicine
[4]Skaggs School of Pharmacy and Pharmaceutical Sciences
University of California, San Diego, 9500 Gilman Drive, La Jolla, CA 92093, USA
[5]Boston Children's Hospital, 300 Longwood Avenue, Boston, MA 02115, USA
[6]Present address: Medical Microbiology, University Medical Center Utrecht, Heidelberglaan 100, 3584 CX Utrecht, The Netherlands
[7]Present address: Division of Biomedical Science, University of California, Riverside, 900 University Avenue, Riverside, CA 92521, USA
*Correspondence: ebier@ucsd.edu
http://dx.doi.org/10.1016/j.chom.2013.08.001

SUMMARY

Cholera toxin (CT), a virulence factor elaborated by *Vibrio cholerae*, is sufficient to induce the severe diarrhea characteristic of cholera. The enzymatic moiety of CT (CtxA) increases cAMP synthesis in intestinal epithelial cells, leading to chloride ion (Cl^-) efflux through the CFTR Cl^- channel. To preserve electroneutrality and osmotic balance, sodium ions and water also flow into the intestinal lumen via a paracellular route. We find that CtxA-driven cAMP increase also inhibits Rab11/exocyst-mediated trafficking of host proteins including E-cadherin and Notch signaling components to cell-cell junctions in *Drosophila*, human intestinal epithelial cells, and ligated mouse ileal loops, thereby disrupting barrier function. Additionally, CtxA induces junctional damage, weight loss, and dye leakage in the *Drosophila* gut, contributing to lethality from live *V. cholerae* infection, all of which can be rescued by Rab11 overexpression. These barrier-disrupting effects of CtxA may act in parallel with Cl^- secretion to drive the pathophysiology of cholera.

INTRODUCTION

Vibrio cholerae (*V.c.*) produces the virulence factor cholera toxin (CT), which alone can cause the severe watery diarrhea pathognomonic of cholera (De Haan and Hirst, 2004; Sack et al., 2004). CT binds to the GM1 ganglioside receptor of intestinal epithelial cells and is then endocytosed and transported in a retrograde fashion to the endoplasmic reticulum, whereupon the enzymatically active A subunit (CtxA) is translocated into the cytoplasm. There, CtxA binds the host cofactor GTP-ARF6 and transfers ADP-ribose from NAD to the α subunit of the stimulating G protein (Gsα) to activate Gsα, which in turn stimulates host adenylate cyclases (ACs) at the plasma membrane, causing a pathological rise in cAMP concentration.

cAMP promotes fluid secretion from crypt intestinal cells primarily by activating cAMP-dependent protein kinase A (PKA), which phosphorylates several ion channels and transporters including the linchpin CFTR chloride ion channel (Cheng et al., 1991; Picciotto et al., 1992), basolateral K+ ion channels, and an ATP-dependent Na^+/K+/Cl^- cotransporter. These combined effects of PKA provoke massive secretion of Cl^- ions into the intestinal lumen. Na^+ ions flow into the lumen via a paracellular pathway to balance the charge of Cl^- ions, thus resulting in a net efflux of NaCl into the gut. Luminal flow of electrolytes produces an osmotic gradient entraining compensatory water efflux, resulting in large volume fluid loss (up to 10–20 l per day). This model of CtxA action is supported by a wealth of experimental evidence, a definitive example being the failure of purified CT to induce fluid secretion in the small intestine of *CFTR*$^{-/-}$ null mutant mice (Gabriel et al., 1994).

Recently, we found that edema factor (EF), a highly active AC (Leppla, 1982) produced by *Bacillus anthracis* (*B.a.*), disrupts endocytic trafficking of adhesion and signaling proteins to adherens junctions (AJs, Figure 1A) (Guichard et al., 2010). This study revealed that EF reduces levels of Rab11, a small GTPase residing in late recycling endosomes which binds to Sec15, a component of the exocyst complex, to tether recycling vesicles to the plasma membrane (Figure 1B; reviewed in Heider and Munson, 2012). Inhibition of Rab11 leads to decreased junctional accumulation of Sec15 and cargo proteins including cadherins (Langevin et al., 2005; Murthy and Schwarz, 2004; Murthy et al., 2010) and Notch pathway components such as the Delta ligand (Guichard et al., 2010; Jafar-Nejad et al., 2005) in flies and in human vascular endothelial cells (Guichard et al., 2010).

Here, we show that CtxA also disrupts Rab11-dependent protein trafficking to cell junctions in *Drosophila* wing and intestinal epithelial cells, in human intestinal epithelial cell lines, and in vivo in ligated murine ileal loops. CtxA also disrupts intestinal barrier integrity in *Drosophila* and contributes to the lethality of live *V.c.*

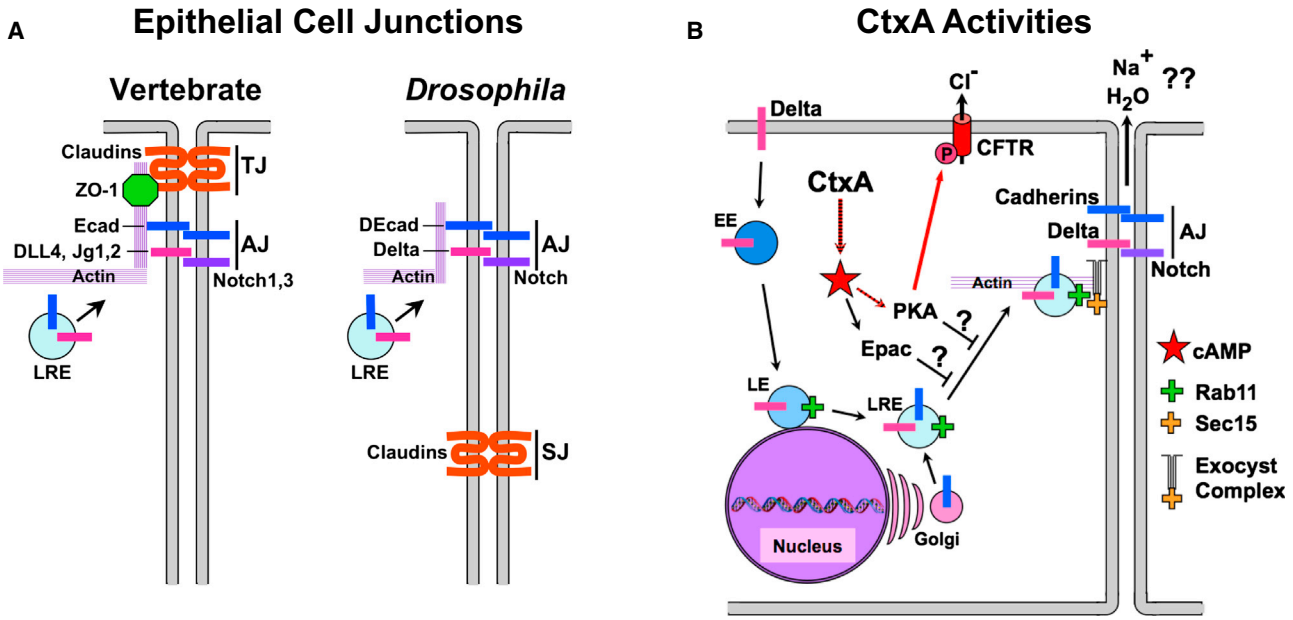

Figure 1. Diagram of Cell-Cell Junctions

(A) Schematic diagram of epithelial cell-cell junctions in vertebrates (left) and invertebrates (right). TJ, tight junction; AJ, adherens junction; SJ, septate junction (the invertebrate functional equivalent of the TJ).

(B) Effect of CtxA and high-level cAMP production in epithelial cells. Notch ligands (e.g., Dl) are endocytosed, and Rab11+ late recycling endosomes (LREs) fuse with Golgi vesicles containing newly synthesized protein cargo (e.g., E-cad). LREs are tethered to the exocyst complex at the plasma membrane via an interaction between Rab11 and Sec15 to initiate delivery of adhesion proteins (e.g., Ecad) and signaling components (e.g., Dl) to the AJ. CtxA leads to overproduction of cAMP to promote PKA-mediated Cl^- secretion via the CFTR ion channel. CtxA also blocks exocyst-mediated trafficking via the PKA and Epac cAMP effectors to disrupt cell junctions (this study). Figure 1 is related to Figure S1.

infection. Importantly, the effects of CtxA can be reversed by overexpression of Rab11. This previously undescribed activity of CtxA, acting in conjunction with its known induction of Cl^- ion secretion, may contribute to the pathophysiology of severe cholera.

RESULTS

CtxA Disrupts Exocyst-Mediated Junctional Trafficking in *Drosophila* Epithelial Cells

CtxA activates Gsα pathways in the early *Drosophila* embryo (Morize et al., 1998) and wing (Katanayeva et al., 2010). Also, flies infected with *V.c.* die in a *CtxA*-dependent fashion through a process involving host cAMP-regulated ion channels (Blow et al., 2005). To explore CtxA activity in *Drosophila* further, we expressed CtxA directly within the cytoplasm using the heterologous GAL4/UAS gene expression system (Brand and Perrimon, 1993), bypassing receptor binding and endocytic steps involved in host cell entry. In the well-characterized wing developmental system, strong expression of CtxA produced adult phenotypes similar to those observed in Notch mutants, consisting of thickened veins (Figure 2B; compare to wild-type [WT] in Figure 2A) and notches along the wing edge (margin) (see Figure S1B online, arrow, compare to mild N^-/+ phenotype in Figure S1A). Furthermore, CtxA reduced expression of the Notch target gene *cut* (Figure 2E, compare to Figure 2D) along the wing margin primordium. Consistent with CtxA acting via the expected Gsα-mediated activation of endogenous AC in the wing, coexpressing CtxA with either of two *Drosophila* Gsα subunits caused wing phenotypes that were much stronger than those produced by CtxA alone (Figures S1G–S1L). Also, expression of a constitutively active form of one of these Gsα subunits (Gsα60A) mimicked the effect of CtxA (Katanayeva et al., 2010). Reciprocally, RNAi knockdown of genes encoding any of three Gsα subunits (Figures S1M–S1R) or the AC *rutabaga* (Figures S1S and S1T) markedly suppressed CtxA phenotypes.

Genetic epistasis experiments confirmed the Notch inhibitory activity of CtxA. For example, an activated allele of *Notch* (*N**) fully suppressed the effect of CtxA (Figure S1E, compare to Figures S1A and S1D), indicating that CtxA acts upstream of the Notch receptor. Conversely, CtxA reversed the vein-loss phenotype caused by ectopic expression of the Delta ligand in the second wing vein primordium (Figure S1F), revealing that it acts downstream of ligand production. In addition, the thickened veins of CtxA-expressing wings were significantly enhanced in *Notch*−/+ heterozygotes (Figure S1C).

CtxA-induced wing phenotypes are highly similar to those produced by a dominant-negative (DN) version of Rab11 (Figure 2C, compare to Figure 2B), a small GTPase involved in recycling endocytic vesicles to AJs. Consistent with their closely allied adult wing phenotypes, CtxA and DN-Rab11 both reduced expression of the Notch target gene *cut* along the presumptive wing margin in imaginal discs (Figures 2D–2F). CtxA and DN-Rab11 acted synergistically when coexpressed (Figure 2I, compare to Figures 2B and 2C), while coexpression of WT-Rab11 (which on its own had no visible effect—Figure 2G) with CtxA almost fully rescued

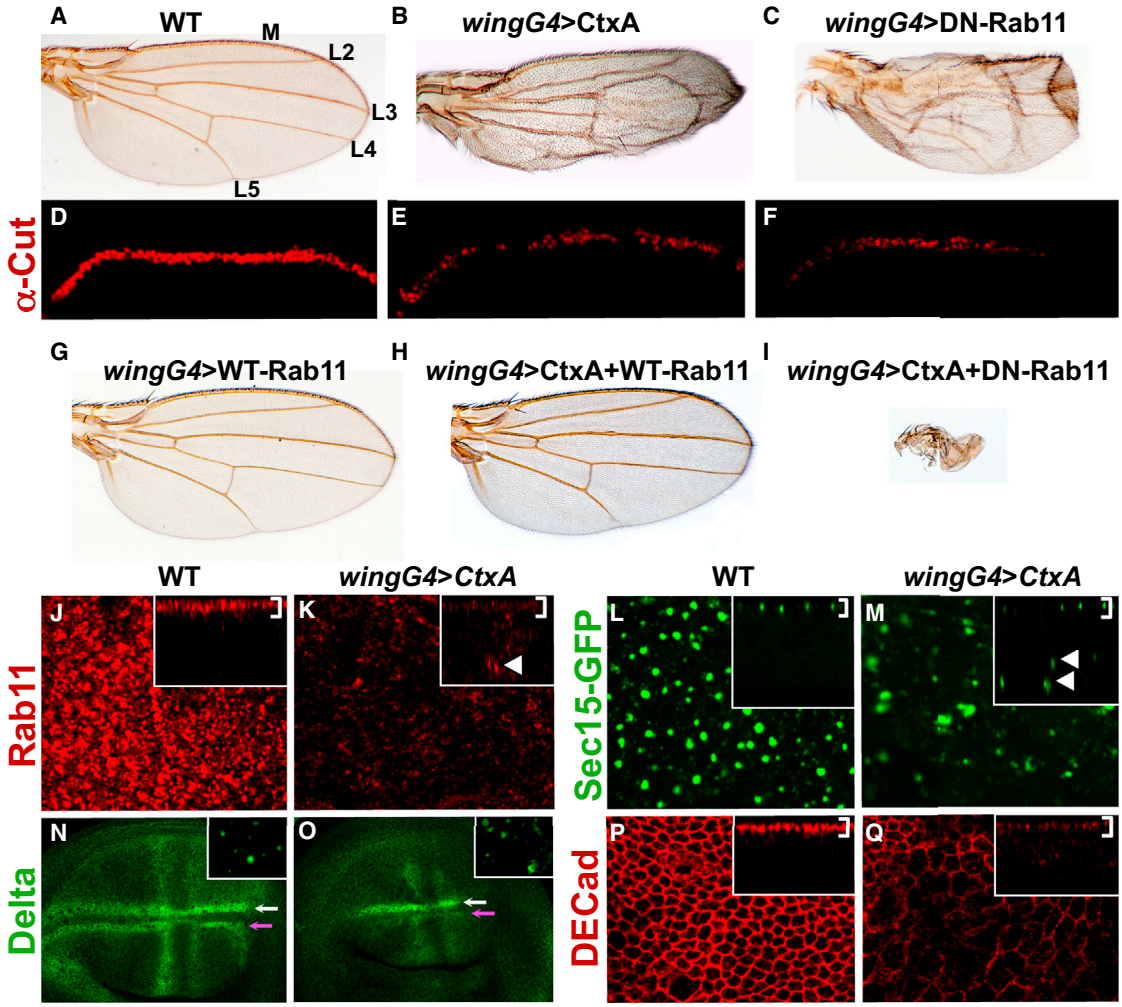

Figure 2. CtxA Inhibits Notch Signaling and Rab11 Activity in *Drosophila*

(A–C, G–I) *Drosophila* wings of the indicated genotypes. Longitudinal veins = L2–L5; wing margin = M. (D–F) Expression of the Notch target gene *cut* (detected by anti-Cut staining) along the margin in third-instar larval imaginal discs of the indicated genotypes. (J, L, N, and P) WT wing discs, and (K, M, O, and Q) wing discs expressing CtxA under the control of the *wingGAL4* driver stained for expression of exocyst (Rab11, Sec15-GFP) and AJ (Delta, DECad) components. Larvae were raised at 25°C for all panels, except (P) and (Q) were raised at 29°C for 3 hr prior to dissection. Insets in (J)–(Q) are z sections. Insets in (N) and (O) are deeper horizontal sections. Arrows in panels in (N) and (O) indicate the two parallel rows of cells giving rise to the dorsal (magenta) and ventral (white) components of the wing margin. The *wingGAL4* driver is expressed more strongly on the dorsal surface, consistent with the effects of CtxA expression being more pronounced on the dorsal component of the margin (O). Arrowheads in (M) indicate ectopic basal vesicles. Figure 2 is related to Figure S2.

the toxin phenotype (Figure 2H, compare to Figure 2B). Moreover, CtxA significantly reduced apical levels of Rab11 (Figures 2J and 2K) and resulted in basal mislocalization of this GTPase (Figure 2K, arrowhead in inset). CtxA also greatly reduced the levels of a GFP-tagged form of Sec15 (Figure 2M), the exocyst binding partner of Rab11, which normally appears within large round structures near the apical cell surface (Figure 2L). In CtxA-expressing cells most remaining Sec15-GFP vesicles appeared irregular in shape and were mislocalized more basally (Figure 2M, arrowheads in inset). These alterations in Rab11/Sec15 levels and distribution were associated with expected defects in endocytic recycling of cargo such as the Notch ligand Delta (Figures 2N and 2O) and the cell adhesion molecule DECad (Figures 2P and 2Q) to AJs. Reflecting the potent Rab11 rescue of the adult CtxA wing phenotype (Figure 2H), apical Sec15-GFP vesicles and junctional levels of Delta and DECad were nearly fully restored by coexpression of Rab11 with CtxA (Figures S2C–S2H). We conclude that CtxA inhibits exocyst-mediated trafficking of DECad and Delta to cell junctions in *Drosophila* wing epithelial cells.

CT Disrupts Cell-Cell Junctions and Notch Signaling in Human Intestinal Epithelial Cells

We next asked whether CT treatment of human intestinal epithelial cells could disrupt trafficking to junctions as CtxA expression did in flies. We treated newly confluent cultures of CACO-2 or T84 cells with purified CT (CtxA/B) and examined the localization of Rab11, Sec15, and candidate cargo proteins at cell-cell junctions (Figure 3). Well-defined AJs form in untreated CACO-2 cells, which are delineated by apically restricted E-cadherin

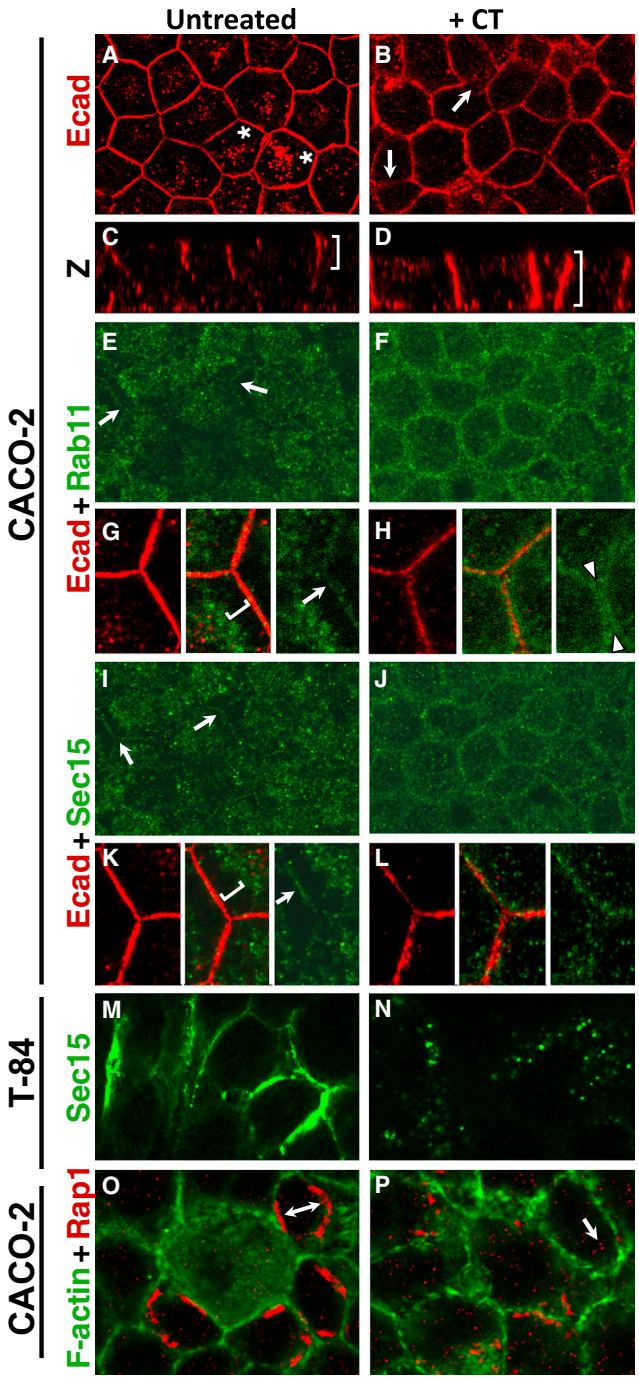

Figure 3. CT Disrupts Localization of Exocyst and AJ Components in Human Intestinal Epithelial Cells

Expression of exocyst and AJ components in recently confluent monolayers of CACO-2 cells (A–L, O, and P) and T84 (M and N) cells either untreated or CT treated (three times over a 28 hr period). (A–D) Ecad viewed from above (A and B) or in cross section (C and D). A prominent cytoplasmic pool of Ecad vesicles is present only in untreated cells (A, asterisks). Ecad is mislocalized along the entire apicobasal axis of CT-treated cells (C and D, brackets). (E–L) The same field of cells triple stained for Rab11 (green), Sec15 (green), and Ecad (red). Arrows highlight narrow bands of Rab11 or Sec15 membrane-adjacent staining, which colabels with Ecad (G and K, center panels) and are separated from a pool of cytoplasmic staining by a subcortical zone virtually devoid of labeling (brackets in G and K). In contrast, CT-treated cells display a clear gap between Rab11/Sec15 staining from neighboring cells that corresponds to the position of Ecad staining (H, right panel, arrowheads). (O and P) Localization of the EPAC effector Rap1 to points of cell-cell contact in a subset of cells (double arrow) is largely disrupted in CT-treated cells, which have more labeled small cytoplasmic vesicles (arrow). Figure 3 is related to Figure S3.

(Ecad) staining (Figures 3A and 3C). In these cells, Rab11 (Figures 3E and 3G) and Sec15 (Figures 3I and 3K) accumulate in a grainy cytoplasmic pool and are enriched within a narrow apical band colocalizing with the AJ (arrows in Figures 3E and 3G, Rab11; and Figures 3I and 3K, Sec15).

Reduced junctional levels of these components and altered distributions of their protein cargo were evident after 6 hr of CT treatment (data not shown) and became more pronounced in cells treated three times over the course of 28 hr (henceforth our standard regimen). The distribution of core AJ component Ecad was dramatically altered in CT-treated cells, leading to gaps in staining (Figure 3B, arrows; compare to Figure 3A) and loss of its apical restriction, with staining extending along the entire apicobasal axis (Figure 3D, compare to Figure 3C). In addition, a cytoplasmic pool of Ecad present in untreated cells (Figure 3A, asterisks) virtually disappeared in CT-treated cells (Figure 3B). CT also abolished junctional localization of Rab11 (Figures 3F and 3H; compare to Figures 3E and 3G) and Sec15 (Figures 3J and 3L; compare to Figures 3I and 3K) and caused ectopic accumulation of these proteins in subcortical regions (Figures 3F and 3J; compare to Figures 3E and 3I), which are zones virtually devoid of Rab11 and Sec15 label in untreated CACO-2 cells (brackets in Figures 3G and 3K). Similarly, in T84 cells, Sec15 staining at the cell surface, which in some cells was very pronounced (Figure 3M), was greatly diminished by CT treatment (Figure 3N), and the remaining Sec15 staining was observed in scattered cytoplasmic vesicles.

Transmission electron microscopy (EM) of CT-treated CACO-2 cells revealed prominent varicose gaps between cells and disorganized convoluted junctions (Figures 4A and 4B), which were paralleled by broadened and less-uniform subcortical F-actin staining (Figures 4C and 4D; arrows indicate tricellular varicosities in Figure 4D; see also Figures S3C and S3D). However, CT did not appreciably alter the apical meshwork of tubulin fibers (Figures S4A–S4D), indicating that the cytoskeletal architecture was not globally disrupted.

We also examined the structure of tight junctions (TJs) following CT treatment. In untreated CACO-2 cells, the TJ adhesion protein claudin-2 (Cld2), which serves as a major paracellular cation and water pore in the intestinal epithelium (Rosenthal et al., 2010), is localized to a narrow apical band (Figure 4E). However, in CT-treated cells, Cld2 staining followed a convoluted path with abnormal cytoplasmic accumulations (Figure 4F, arrows), and overall Cld2 levels were markedly increased compared to untreated cells (compare insets in Figures 4E and 4F). Similarly, normally continuous staining of the TJ adaptor protein ZO-1 (Figures 4G and 4K) assumed a tortuous path and accumulated in large patches along the borders of CT-treated cells (Figures 4H and 4L). While CT treatment resulted in a net increase in ZO-1 staining, junctional levels of ZO-1 remained normal and restricted to the apical region of the cell (Figures 4I and 4J; Figures S4C and S4D), contrasting with mislocalization of the AJ protein Ecad that spanned the apicobasal axis

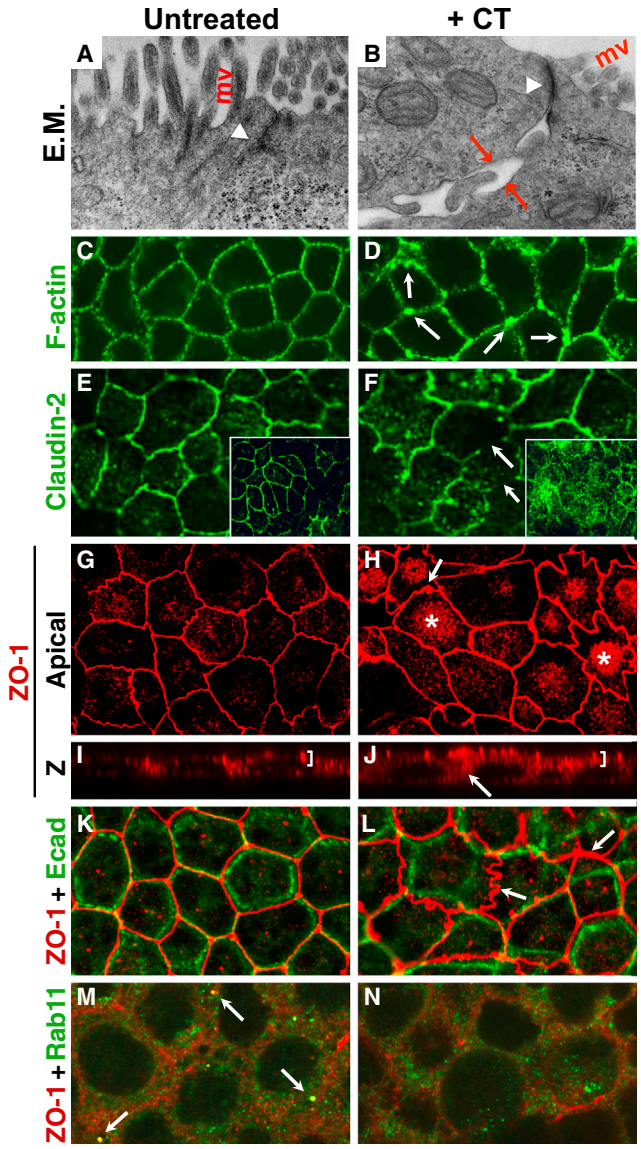

Figure 4. CT Disrupts Localization of TJ Components in Intestinal Epithelial Cells

Expression of TJ components in untreated (A, C, E, G, I, K, and M) and CT-treated (B, D, F, H, J, L, and N; three times over 28 hr) recently confluent CACO-2 cells fixed in paraformaldehyde, except for (K) and (L) (methanol fixed). (A and B) Electron micrographs of untreated CACO-2 cells (A) and CT-treated cells (B), in which prominent gaps (arrow) and convoluted borders are visible between cells, which can span a significant fraction of the apicobasal axis. Apical junctions (arrowheads) also tend to be less regular in CT-treated cells, and microvilli (mv) are reduced. CT treatment disrupts regularly spaced cortical F-actin fibers (C), resulting in broader and disorganized phalloidin staining (D, arrows). Continuous staining of the TJ protein Claudin-2 (E) is interrupted in CT-treated cells (F, arrows). Regular ZO-1 staining (G) becomes irregular in CT-treated cells, punctuated by varicose accumulations (H, arrow), and ZO-1 staining accumulates in the cytoplasm, which in some cells forms a cap over the nucleus (H, asterisks). (I and J) z section of ZO-1 stains. Bracket, apical region; arrow, ectopic basal ZO-1. The registration of the TJ and underlying AJ (K) collected from adjacent focal planes is uncoupled in CT-treated cells (L, arrows). (M and N) ZO-1 and Rab11 colocalize in a subset of large vesicles adjacent to the plasma membrane (M, arrows) which is lost following CT treatment (N). Figure 4 is related to Figure S4.

(Figures 3C and 3D). The most prominent increase in ZO-1 levels was in a basally located cytoplasmic pool (Figure S4D) and in a bright disk above the nucleus in some CT-treated cells (Figure 4H, asterisks). CT also disrupted the normal close alignment of AJ and TJ components. In untreated cells, these two junctions are closely stacked atop of one another (Figure 4K, red apical ZO-1 and green AJ-level Ecad staining), a feature lost in CT-treated cultures. In some cases, the TJ path ran entirely out of register with that of the underlying AJ border (Figure 4L, arrows). These effects of CT on the TJ were most pronounced in newly confluent cells but also evident in mature confluent monolayers (Figures S4E–S4H). Paralleling effects observed with ZO-1, CT induced an irregular pattern of occludin staining at cell borders as well as ectopic foci of cytoplasmic accumulation (Figures S4I–S4L). Finally, CT disrupted a vesicular association of Rab11 with ZO-1. In untreated CACO-2 cells, a subset of large Rab11 vesicles colocalized with ZO-1 just below the level of the TJ (Figure 4M, arrows), suggesting that Rab11-dependent endocytic recycling aids in trafficking this adaptor protein to cell-cell junctions. Such colocalization of Rab11 with ZO-1 was virtually abolished in CT-treated cells (Figure 4N). Similarly, in T84 cells, Rab11 and ZO-1 colocalized in large vesicles (Figure S4O), and this association was greatly reduced by CT treatment (Figure S4P). As in CACO-2 cells, high levels of ZO-1 also accumulated ectopically in basal regions of CT-treated T84 cells (Figure S4R, arrows; compare to Figure S4Q).

Since CtxA reduced Delta trafficking to the AJ and inhibited Notch signaling in *Drosophila*, we also examined the distribution of Notch pathway components in CACO-2 cells. Notch ligands Delta-like 4 (Dll4) and Jagged-2 (Jg2) and receptor Notch-3 (N3) are primarily detectable in punctate vesicles located in close proximity to the plasma membrane (Figures 5A, 5C, and 5E). In contrast, all Notch components exhibited a diffuse spongy cytoplasmic staining pattern in CT-treated cells (Figures 5B, 5D, and 5F). The CT effect was particularly pronounced in a subset of newly confluent CACO-2 cells, which formed scattered circular cup-like structures with rims delineated by F-actin (Figures S3G–S3J). In untreated cells, Notch pathway components accumulated along the inner lip of these cups, forming rings of high-level staining (Figures S5A, S5C, and S5E). CT treatment eliminated this staining and disrupted the radial symmetry of these cup-like structures (Figures S5B, S5D, and S5F). Consistent with its effects on localization of Notch pathway components, CT greatly reduced levels of signaling via the Notch1 receptor. Following ligand binding and receptor proteolysis, an activated cleavage product of the receptor (N1*) translocates to the nucleus and acts as a transcriptional cofactor to regulate expression of Notch target genes (Fortini, 2009). In untreated cells, the great majority of N1* staining was confined to the nucleus (Figure 5G), reflecting constitutive signaling via this receptor. Following CT treatment, nuclear N1* staining was greatly reduced (Figure 5H), indicating strong inhibition of this pathway.

cAMP exerts its effects through two known effectors, PKA and Epac (a guanine nucleotide exchange factor that activates the small GTPase Rap1). We asked whether these two major cAMP effector branches mediated the junction-disrupting effects of CtxA. In CACO-2 cells, inhibitors specific for PKA (H89) or Epac (ESI-09) markedly reduced CT effects (Figures

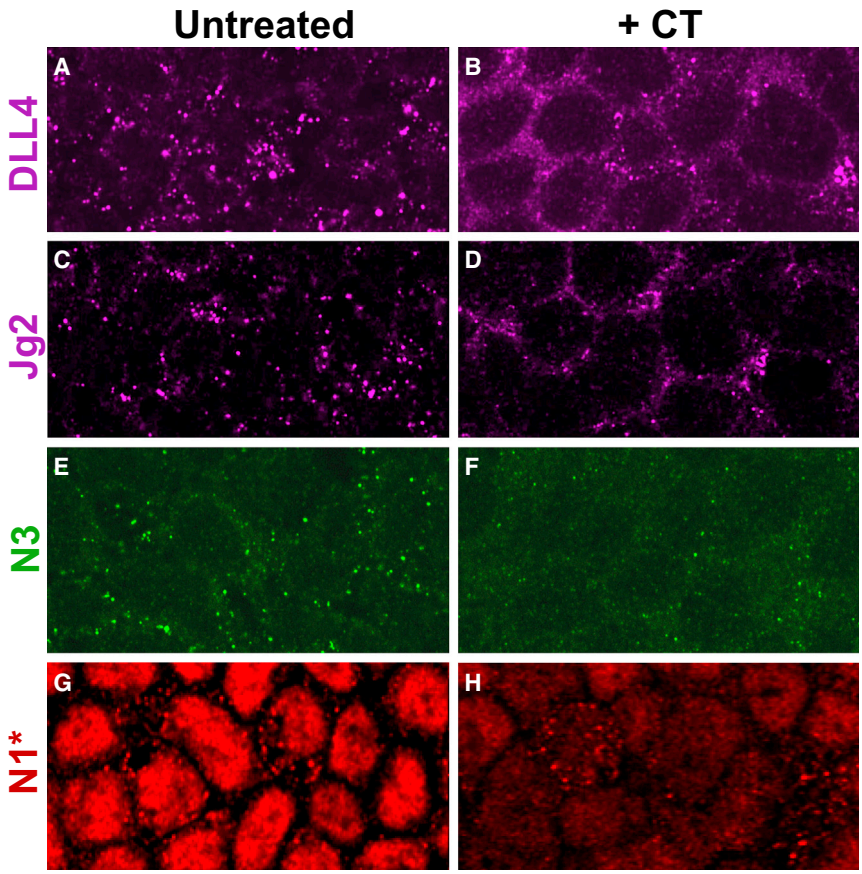

Figure 5. CT Disrupts Localization of Notch Pathway Components and Signaling

Recently confluent monolayers of CACO-2 cells, untreated or treated with CT (three times over 28 hr), were fixed with paraformaldehyde and stained for expression of the Notch pathway components as indicated. N1*, activated Notch1. The equalization of nuclear and cytoplasmic N1* staining observed here is also observed in cells treated for only 6 hr with CT in which the overall levels of staining have not yet been greatly diminished. Figure 5 is related to Figure S5.

S5G–S5J), while cAMP analogs that selectively activate PKA (6Bnz, Figure S5K) or Epac (8Cpt, Figure S5L) mimicked CT-induced junction disruption assessed by ZO1 staining at TJs and Ecad staining at AJs (data not shown). Consistent with CT acting on the Epac cAMP-effector branch, CT-treated cells displayed reduced subcortical localization of the Epac mediator Rap1 (Figures 3O and 3P). Paralleling these human cell results, expression of activated forms of PKA (PKA*) or Rap1 (Rap1*) in the *Drosophila* wing epithelium mimicked the effect of CtxA, including adult wing phenotypes (Figures S2I–S2K) and reduced levels of Rab11 (Figures S2L–S2N), Sec15-GFP (Figures S2O–S2Q), and Delta (Figures S2R–S2T).

CT Reduces Levels of Exocyst Components in Ligated Murine Ileal Loops

We next examined whether CT reduced levels of endocytic recycling components and disrupted cell-cell junctions in vivo employing the ligated murine ileal loop model. In anesthetized mice, two segments of the small intestine (ileum) were ligated with bowel clamps. CT was then injected into one of the segments and control saline into the other. The ligated intestines were returned to the body cavity, the incisions sutured, and the animals kept anesthetized for an additional 5 hr before sacrifice. While control ileal loops appeared similar to adjacent nonligated segments of the intestine (Figure 6A), CT-treated segments were markedly inflated (Figure 6B, and quantified in the Experimental Procedures), indicative of the classic fluid secretion associated with CT intoxication.

In uninjected mice or control ileal loops injected with saline, strong Rab11 staining was detected as an uninterrupted apical band running along the luminal epithelial surface of the crypt-to-villus axis (Figures 6C and 6E), consistent with previous descriptions (Goldenring et al., 1996; Silvis et al., 2009). In tangential sections at the level of the crypts, Rab11 staining appeared as circular luminal rings (Figure 6E). Sec15 staining was primarily confined to large cytoplasmic vesicles in the crypts (Figure 6G), with much lower levels detected in the villus. In CT-injected loops, the staining for these endocytic trafficking components was dramatically reduced. Apical Rab11 staining virtually disappeared along the entire crypt-villus axis (Figures 6D and 6F), and cross-sections of the crypts were less circular than in controls (Figure 6F, arrows). Similarly, Sec15 staining was greatly reduced in a subset of crypts (Figure 6H) that received high levels of CT (Figure S6), which were also irregularly shaped. Paralleling the effects we observed in CACO-2 cells (Figures 3C and 3D), CT induced a redistribution of Ecad in vivo. In untreated ileal loops, Ecad was concentrated apically at AJs (Figure 6K, arrows) and accumulated in a prominent cytoplasmic pool (Figure 6K, asterisks). In contrast, in CT-treated loops, Ecad staining expanded to occupy the entire apicobasal axis with a concomitant reduction of the cytoplasmic pool (Figure 6L, asterisks). In addition, Ecad staining often forked apically in CT-treated loops (arrows in Figure 6L, compare to 6K), revealing a clear separation between adjacent cells, evident also by apical gaps in F-actin staining (arrows in Figure 6J, compare to smooth apical surface contour in Figure 6I). Leakage of albumin from the vasculature into the intestinal lumen has been reported in human cholera patients (in the rice stool) as well as in CT-treated rabbits (De and Chatterje, 1953). Similarly, we found that elevated levels of albumin staining accumulated adjacent to the luminal surface of some CT-treated crypts as well as within the lumen itself (Figures 6M and 6N). We conclude that CT reduces endocytic trafficking in vivo in the small intestine, causing junctional defects similar to those observed in cell culture and leading to leakage of fluid and protein into the intestinal lumen.

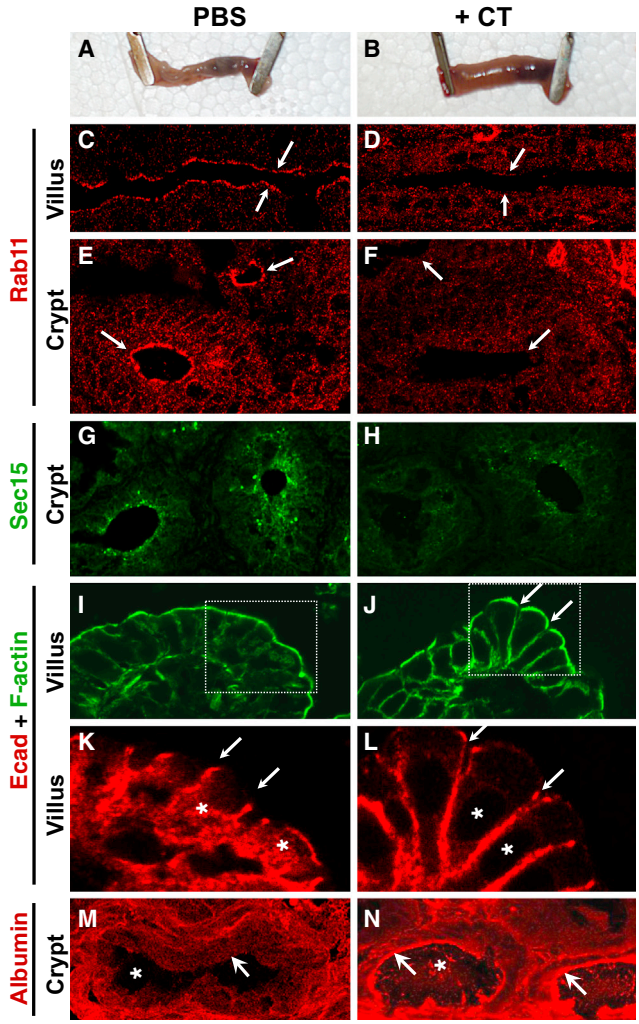

Figure 6. CT Disrupts Localization of Exocyst Components In Vivo in Ligated Ileal Loops

Ligated ileal loops injected with saline (A) or CT (B) and incubated for 5 hr. Rab11 staining in control loops (C and E) resembles that of nontreated animals (data not shown), localizing to a narrow apical region (arrows) in epithelial cells of both the villus (C) and crypt (E), which is virtually abolished in CT-injected loops (D and F). Crypts in CT-injected loops are also less regularly shaped than in controls (E and F). Apical Sec15 staining in the crypts of control loops (G) is greatly reduced in CT-injected loops (H). Regular F-actin staining in untreated control loops (I) becomes irregular and discontinuous (arrows) in CT-treated loops (J). Apical E-cadherin (Ecad) staining (arrows) is tightly aligned between neighboring epithelial cells in control injected loops (K) but often forks apically in CT-treated loops (L, arrows) revealing partial separation between adjacent cells. A cytoplasmic pool of Ecad in untreated epithelial cells (K, asterisks) is virtually abolished by CT treatment (L, asterisks indicate cytoplasmic void in staining). Albumin staining in control crypts, which is excluded from the lumen (M), accumulates at high levels along the luminal face of some crypts (arrow) as well as within the lumen itself (asterisk) in CT-treated injected loops (N). Figure 6 is related to Figure S6.

Elevated Rab11 Protects against CtxA-Dependent *V. cholerae* Infection in *Drosophila*

The *Drosophila* midgut epithelium shares many structural and regulatory mechanisms with the mammalian small intestine and has been widely used as a model for basic cell biological functions including innate immunity, response to damage, and stem cell homeostasis (reviewed in Apidianakis and Rahme, 2011). Furthermore, oral infection of *Drosophila* with *V.c.* results in CT-dependent weight loss and lethality (Blow et al., 2005). We therefore used this system to examine the role of Rab11 in maintaining intestinal barrier function.

Targeted CtxA expression in the *Drosophila* midgut using the NP1 GAL4 driver resulted in emaciated flies (Figure 7B, compare to Figure 7A) with reduced body weight (Figure 7D, Figure S7B), and coexpressing WT-Rab11 with CtxA counteracted these toxic effects (Figures 7C and 7D). In addition, adult-specific expression of Ctx in the midgut reduced viability, an effect also rescued by Rab11 overexpression (Figure S7A). Conversely, reduction in Rab11 levels (i.e., heterozygosity for either of two *rab11*− loss-of-function alleles: see the Experimental Procedures) resulted in midgut CtxA expression becoming 100% lethal (data not shown). Midgut expression of CtxA also reduced apical levels of Rab11 (Figure 7E), Sec15 (Figures 7I and 7J), the AJ markers Ecad (Figures 7L and 7M), and α-catenin (Figures S7D–S7G), and the septate junction marker Polycheatoid (Pyd)—the *Drosophila* ortholog of ZO-1 (Figures S7C–S7E). Ultrastructural analysis revealed that, similar to CT-treated CACO-2 cells, CtxA expression in the *Drosophila* midgut caused significant gaps and convoluted borders between intestinal epithelial cells (Figures 7O and 7P; Figures S7H–S7P). Overexpression of Rab11 rescued these CtxA-induced junctional defects in the midgut, restoring apical staining of Sec15-GFP (Figure 7K) and Ecad (Figure 7N), and reducing the size of gaps between enterocytes evident at the EM level (Figure 7Q). In addition, weight loss caused by midgut expression of CtxA could be rescued by RNAi knockdown of Gsα60A or inhibition of the SK K+ channel with clotrimazole (Figure S7B), both essential for CtxA-dependent weight loss and lethality in flies infected with *V.c.* (Blow et al., 2005). Thus, CtxA acts by very similar mechanisms in *Drosophila* intestinal and wing epithelial cells to disrupt Rab11-dependent junctional trafficking.

Barrier disruption in the gut can also be assessed using a leakage assay in which flies are fed a solution of sugar water containing a colored food dye (Rera et al., 2011). Dye accumulation is restricted to the intestine in 100% of young WT flies, but if the epithelial barrier is breached, dye accesses internal body cavities and appendages, producing blue "smurfing" flies (Rera et al., 2011). In contrast to WT or NP1/+ control flies (Figure 7F), midgut-specific expression of CtxA resulted in a significant fraction (≈20%) of smurfing flies (Figure 7G). Expression of DN-Rab11 in enterocytes (Figure 7H) also caused dye leakage at frequencies comparable to CtxA treatment, indicating that inhibition of endocytic recycling is sufficient to induce barrier disruption in the gut. Unlike CtxA, however, DN-Rab11 did not cause weight loss (data not shown), suggesting that a critical component of CtxA-dependent fluid leakage and weight loss are mediated by a Rab11-independent mechanism, such as cAMP-regulated ion channel activation (Blow et al., 2005).

As previously shown for exogenous CT provided during live infection of *Drosophila* with *V.c.* (Blow et al., 2005), gut-specific expression of CtxA restored lethality upon infection with a *V.c.* Δ*ctxa* mutant (Figure 7R) and also accelerated death caused by infection with the WT strain. Consistent with our model, overexpression of WT-Rab11 increased survival of flies infected with

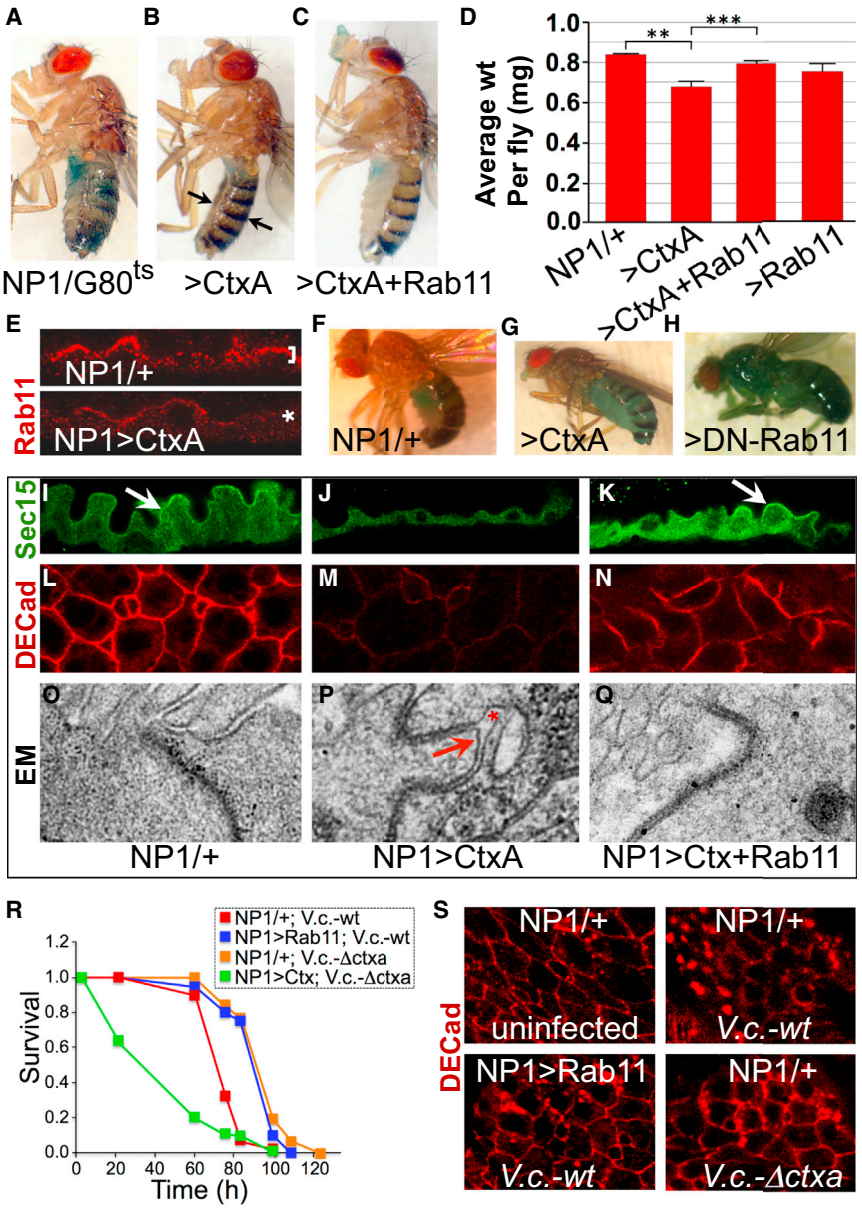

Figure 7. Rab11 Rescues CtxA-Dependent Weight Loss and Junction Disruption in *Drosophila*

(A–C and F–H) Flies were fed a 5% sucrose plus dye solution. (D, E, and I–S) Flies were fed standard solid fly food. Adult NP1-GAL4/tubGAL80ts control flies (A) appear WT. Modest midgut expression of CtxA with this driver in flies raised at 22°C (RT), a permissive temperature for GAL80 that reduces but does not eliminate NP1-GAL4 activity, results in emaciated flies (B, arrows), which is counteracted by coexpression with Rab11 (C). Hindgut-specific expression of CtxA also results in a similar emaciated phenotype (data not shown). (D) Average weights of NP1/GAL80ts control flies and flies expressing CtxA, CtxA+WT-Rab11, or WT-Rab11 alone in the gut (error bars, SD). **p = 0.0017 for the comparison of NP1/G80ts controls versus NP1/G80ts > CtxA flies; ***p = 0.0008 for the comparison of NP1/G80ts > Ctx versus NP1/G80ts > Ctx+Rab11. (E) Apical Rab11 staining in the midgut of an NP1/+ control fly bracket in upper panel) is reduced by CtxA expression (asterisk in lower panel). (F–H) Flies were fed with a sucrose dye solution, which remains strictly confined to the intestine in WT flies (F) but leaks into the body cavity of "smurfing" flies expressing CtxA (G) or DN-Rab11 (H) in the midgut. (I–Q) Junction-disrupting effects of CtxA can be rescued by coexpression with Rab11. Note: the DECad-Tomato construct is expressed from the endogenous DECad promoter. Sec15 indicates Sec15-GFP which was detected by an anti-Sec15 antibody. (R) Infection of flies with a Δ*ctxa* strain of *V. cholerae* (*V.c.*, orange curve) results in decreased lethality compared to infection WT *V.c.* (red curve, $p < 0.0001$), and midgut specific expression of CtxA (with the NP1 GAL4 driver) restores lethality (green curve, $p < 0.0001$) to the *V.c.* Δ*ctxa* strain. (S) Rab11 rescues CtxA-dependent junction disruption caused by infection of flies with *V.c.*. DECad, DECad-Tomato. (T) Summary model. Figure 7 is related to Figure S7.

DISCUSSION

In the current study, we find that CtxA causes emaciation, disorganized junctions, and barrier disruption when expressed in the *Drosophila* midgut and contributes to lethality during infection of flies with *V.c.* Similarly, CT treatment produced apical gaps between epithelial cells in murine ileal loops, and histochemical staining and ultrastructural examination of CT-intoxicated human CACO-2 cells and *Drosophila* intestinal epithelial cells reveal parallel pathologies consisting of intercellular lacunae and convoluted borders between cells virtually identical to those observed in duodenal biopsies from human cholera patients (Mathan et al., 1995). Also, increased epithelial dye permeability has been reported in rats, mice, and rabbits following CT exposure (Magnusson et al., 1985; Ohishi and Odagiri, 1984; Triadafilopoulos et al., 1989), and serum albumin was *V.c.* (Figure 7R). Paralleling the effects of directly expressing CtxA in the midgut (e.g., in NP1 > Ctx flies), *V.c.* infection of flies resulted in *ctxA*-dependent downregulation of junctional Ecad levels (Figure 7S), once again rescued by overexpression of Rab11 (Figure 7S). Cumulatively, these findings implicate Rab11-dependent endocytic recycling in maintaining normal intestinal barrier function and indicate that boosting this process offers protection against CT-dependent effects of *V.c.* infection.

found in the lumen of CT-treated rabbit ileal loops and in the stool of some cholera patients (De and Chatterje, 1953), which we too observed in CT-treated murine ileal loops. Furthermore, subcutaneous injection of CT in guinea pigs and rabbits leads to vascular effusion (Craig, 1965), which has been used as a criterion for assessing virulence of *V.c.* isolates (Sasmal et al., 1995).

Both CT and EF inhibit junction formation and barrier function at least in part by inhibiting Rab11-dependent endocytic recycling. Thus, overexpression of WT-Rab11 in the gut rescued CT-induced weight loss, junctional organization, and intestinal barrier integrity in *Drosophila* as well as CT-dependent sensitivity to *V.c.* infection. Interestingly, gut-specific inhibition of Rab11 alone did not result in weight loss, suggesting that the activation of ion channels is Rab11 independent (Blow et al., 2005). Cumulatively, these data provide strong evidence for a junction-destabilizing effect of CT, which may act in concert with known toxin effects to stimulate fluid loss.

Potential Role of Junction Disruption by CtxA with Regard to Its Effects on Ion Secretion

A large body of work has established that CT-dependent cAMP production activates PKA, which then phosphorylates and increases the conductance of the apically localized CFTR, a Cl^- ion transporter concentrated in epithelial cells of crypts in the small intestine (Jakab et al., 2011; Strong et al., 1994). The resulting Cl^- flux is accompanied by efflux of Na^+ ions and water into the intestinal lumen to preserve charge and osmotic balance, respectively. The exact path by which Na^+ and water flow across the epithelium is not certain, but it is generally assumed that at least part of this flux occurs via the paracellular route (Barrett, 2006; Frömter and Diamond, 1972; Pappenheimer and Reiss, 1987). The ability of CT to inhibit endocytic recycling and disrupt epithelial junctions reported here could contribute to fluid secretion in several ways. First, by disrupting the highly regulated organization of the junctions, the paracellular flow of cations and water might be facilitated in the crypts where CT strongly downregulated Rab11 and Sec15 and expression of the CFTR Cl^- channel is maximal. Our observation that serum albumin accumulates within the lumen of crypts in CT-treated ileal loops is consistent with such compromised junctional barrier integrity. Second, elevated levels of Cld2, a paracellular channel selective for cations and water (Rosenthal et al., 2010), could contribute to increasing Na^+ conductances, as suggested by a recent study in which Notch inhibition in CACO-2 cells led to elevated levels of Cld2 and increased epithelial conductances (Dahan et al., 2011). In the villus, CT may also destabilize junctions as it reduced Rab11 levels along the entire axis, altered expression of Ecad, and induced apical gaps.

CT inhibition of exocyst-mediated recycling could also alter the dynamics of ion channel turnover or targeting to the apical and basal membranes. Indeed, Rab11 has been implicated in recycling of CFTR in the crypt (Silvis et al., 2009). The degree to which such potential perturbations in trafficking of ion channels might contribute to the overall effect of CT in the intestinal epithelium merits further examination.

In addition, the exocyst is involved in secretion of various factors, and therefore its inhibition by CT could alter release of cytokines from immune cells or endocrine intestinal epithelial cells, which normally contribute to regulating fluid balance via the enteric nervous system and submucosal immune cells (Lundgren, 2002). For example, Rab11 has recently been shown to be required for secretion of the permeability signals TNF-α and IFNγ from natural killer T cells (Reefman et al., 2010).

Disruption of Cell-Cell Junctions by cAMP-Producing Toxins

The junction-disrupting effects of CtxA in *Drosophila* epithelial cells and in human intestinal cell lines resemble those caused by anthrax EF toxin in human vascular endothelial cells (Guichard et al., 2010), consistent with these toxins acting via the common mechanism of cAMP overproduction. EF toxin decreased TER (Ebrahimi et al., 2011) and increased dye permeability in HBMEC cells, and subepidermal and pulmonary vascular effusion caused by injection of *B.a.* bacteria were found to be EF dependent (Guichard et al., 2010). Since ET also induces the formation of transcellular tunnels in vascular endothelial cells (Maddugoda et al., 2011), it will be interesting to determine if this effect is also exocyst dependent. In the current study, we observed junctional defects mimicking those caused by CT in CACO-2 cells treated with cAMP analogs specific for the primary cAMP effectors PKA and Epac, consistent with a prior report of similar, albeit weaker, effects in cells treated with the broad spectrum cAMP analog 8Br-cAMP (Boucher et al., 2005). Likewise, in *Drosophila*, expression of activated forms of either PKA or Rap1 (the small GTPase activated by Epac) caused wing phenotypes similar to those caused by CT and downregulated junctional Rab11, Sec15-GFP, and Delta. Conversely, the effect of CT in CACO-2 cells was attenuated by specific inhibitors of either PKA or Epac, further supporting a role of both of these cAMP pathways in the junction-disrupting effects of CT.

One interesting aspect of CT action is that it has different effects on the AJ (e.g., reduction in levels of Rab11, Sec15, and Notch components and apicobasal mislocalization of Ecad) versus TJ (e.g., increased junctional levels of ZO-1 and Cld2, which remain apically restricted). CT treatment also uncoupled these two junctional complexes, suggesting that it disrupts a process that normally ensures their close alignment. Consistent with our observations that colocalization of a subpool of Rab11+ vesicles with ZO-1 is disrupted by CT treatment in CACO-2 or T84 cells, the exocyst has been proposed to mediate direct delivery of proteins to the TJ (Hazelett et al., 2011).

Determining how the various effects of cAMP overproduction are integrated to alter barrier integrity and assessing the full contribution of the junctional defects we describe here to the pathogenesis of cholera are important lines of inquiry for future studies.

EXPERIMENTAL PROCEDURES

Drosophila Genetics

The *UAS-CtxA* transgene (see below) was stably transformed into the *Drosophila* genome. Flies carrying the *UAS-CtxA* construct were then crossed to various GAL4 driver stocks to drive toxin expression in specific cells. Timing of GAL4 activity was limited by a temperature-sensitive form of GAL80, which inhibits GAL4 function below 29°C.

Transgenic fly stocks include *UAS-CtxA1 UAS-Flp*/TM6*Tb*, *UAS-Sec15-GFP*/CyO (from H. Bellen), *UAS-Rab11-YFPwt*, *wingG4* = MS1096-GAL4, *prdG4* = *paired*-GAL4, *L2G4* = E-GAL4, NP1-GAL4, the *rab11*− loss-of-function alleles *rab11[93Bi]* and *rab11[j2D1]*, N^- = N^{55e11} and N^* = N^{Ax-1} (available

at the Bloomington *Drosophila* Stock Center or by request), UAS-Pyd-GFP (from A. Fanning), and DECad-tomato (from Yang Hong).

Construction of the UAS-CtxA Transgene

A cDNA was PCR amplified from *V.c.* chromosomal DNA encoding the enzymatically active CtxA1 moiety of CT was inserted into the pUASt vector between the EcoR1 and Not1 sites of the polylinker (details available upon request). The PCR primers used deleted CtxA as the signal peptide, introduced a *Drosophila* Kozak sequence followed by an ATG start codon, and inserted a STOP codon at the junction between the A1 and A2 subunits of CtxA. After confirming the sequence of the cloned cDNA, *CtxA1* sequences were excised with Kpn1 and Spe1 and inserted into the pUASt vector.

Infection of *Drosophila* with *V. cholerae*

MO10, a *V.c.* O139 clinical isolate, and a CT subunit B deletion strain (Δ*ctxa*) were used for *Drosophila* infections. Flies were infected orally as described (Blow et al., 2005). Briefly, 30 male flies were divided among three vials that contained a plug saturated with a 1:10 dilution of an overnight culture. Numbers of dead flies in each vial were recorded at least once each day. Survival curves were constructed, and log rank analysis was used to determine statistical significance.

Dye Ingestion Assay

Flies 4–8 days old were starved for 2 hr in empty vials, then transferred to vials with a Kimwipe soaked with 1.2 ml of a 5% sucrose solution containing green (Yellow 5 and Blue 1, Shilling) food colorant (four drops per 10 ml of sucrose solution). Flies were left on the sucrose dye solution and examined twice daily for presence of dye in the abdomen and entire body cavity.

Immunofluorescence

Drosophila *Wing Imaginal Discs and Midgut*

Immunostaining was performed according to standard protocol (e.g., Cook et al., 2004) using the following antibodies: anti-Dl (clone C594.9B from Developmental Studies Hybridoma Bank - DSHB, 1/500), rat anti-*Drosophila* Rab11 antibody (from R. Cohen, 1/500) or mouse anti-Rab11 (BD Transduction Laboratories, #610656, 1/200), guinea pig anti-Sec15 (from H. Bellen, 1/1000), mouse anti-Cut (DSHB, clone 2B10-c, 1/100), rat anti-DECAD (DSHB, 1/500), rat anti-D-CAT1 (DSHB, 1/500), and rabbit anti-GFP (Invitrogen #A11122, 1/500).

Intestinal Cell Lines

Human CACO-2 or T-84 intestinal epithelial cells were fixed in 4% paraformaldehyde/1× phosphate-buffered saline (PBS) for 30′ at RT or in methanol for 10′ at −20°C (only for Ecad, Sec15, and Rab11 stains in Figures 3A–3L, Ecad/ZO-1 stains of Figures 4K and 4L, and occludin stains), washed in PBT (PBS + 0.1% Triton X-100), blocked in 1% BSA-PBT, and processed for staining according to standard protocols. Antibodies were diluted in 1% BSA-PBT. Junctional anti-E-cad staining was performed with methanol fixation. Antibodies used include rabbit anti-Rab11 (Invitrogen, #715300, 1/200), goat anti-Sec15 (F-15, Santa Cruz, sc-34366, 1/50), rabbit anti-DLL4 (Lifespan, LS-C19035, 1/150), goat anti-Jg2 (N-19, sc-34475), goat anti-N3 (M-20, Santa Cruz, sc-7424, 1/100), rabbit anti-activated Notch1 (Abcam, ab83253, 1/500), mouse anti-Ecad (BD, #610404), 1/50), mouse anti-ZO-1 (Invitrogen, #339100, 1/100), rabbit anti-claudin-2 (Invitrogen, 51-6100, 1/100), rabbit anti-occludin (Invitrogen, 71-1500, 1/100), and mouse anti-Rap1 (BD #610195, 1/100).

Cell Culture and CT Treatment

CACO-2 cells were grown in DME/F12 50/50 (Cellgro CN 10-092-cv) medium supplemented with 10% heat-inactivated fetal bovine serum (FBS), Nu-Serum (BD #355500), and a penicillin/streptomycin mix for ≈1 week (recently confluent cultures) or for ≈3 weeks (fully confluent cultures). T84 cells were grown in the same medium with antibiotics, supplemented with 5% newborn calf serum (NCS, no heat inactivation). For CT treatment, cells were grown in 24-well plates on glass coverslips to subconfluence. CT (100 ng/ml Sigma, C8052, diluted in 500 μl of medium) or 500 μl of control medium was added three times at 12 hr intervals, and cells were fixed 4 hr after the last treatment. Cells were also treated with pharmacological agents following the temporal protocol used for 3× CT treatment including 6-Bnz (BioLog, Cat. B 009-10, 100 μM); 8-Cpt (Tocris, #1645, 5 μM); H-89 (Sigma-Aldrich, #B1427, 10 μM); ESI-09 (BioLog, #B 133, 10 μM).

Ligated Intestinal Loop Assay

A midline laparotomy was performed on two 5-week-old male C57BL6 anesthetized mice, and two ligated intestinal loops (≈2 cm) were prepared in the jejunum of each animal using two double clamps of the intestine. Hanks' balanced salt solution (HBSS) (100 μl) containing Ca^{2+}, Mg^{2+}, and 1 μg of CT holotoxin was injected into one loop obliquely with a 29 gauge needle while HBSS alone was injected into the second loop. Wounds were stitched, and animals were kept anesthetized until euthanization 5 hr after surgery. Loops were excised, measured, and weighed before and after luminal content removal for fluid quantification. The fold increase in extruded fluid in CT versus control loops was calculated per unit length of intestine = fluid secretion (mouse 1, control fluid secretion [mg/mm] = 1.03; CT-induced fluid secretion [mg/mm] = 3.88; mouse 2, control fluid secretion [mg/mm] = 0.85; CT-induced fluid secretion [mg/mm] = 5.13, SE = 1.0, p = 0.03; average = 4.9-fold increase ± 1.13 SEM). Specimens of intestinal loop tissue were collected, flash frozen in liquid nitrogen, and stored at −80°C. One section of each loop was placed in a plastic mold filled with OCT compound (Tissue-Tek, Sakura Finetek, USA) and quickly frozen in 2-methylbutane (Fischer Scientific, USA) with dry ice for immunofluorescence studies. All animal experiments were approved by the UCSD Animal Care Program.

Ileal Tissue Sectioning and Staining

Sections (5 μm) of fixed intestinal tissue were cut in a cryostat at −18°C. Slides were air dried at RT for 30 min after sectioning, blocked with 1% BSA (Sigma #A4503) in PBST washing buffer (PBS, 0.1% Tween 20) for 10 min, washed three times with PBST, fixed for 30 min in Formaldehyde-Fresh Solution (Fisher #SF94-4), and washed three times in PBST. Primary antibodies were incubated overnight (4°C), and slides were washed three times in PBST, incubated with secondary antibodies for 30 min (RT), and washed three times in PBST. Antibodies used were goat anti-Sec15 (F-15, Santa Cruz, sc-34366, 1/10), rabbit anti-Rab11 (Invitrogen, #715300, 1/250), rabbit anti-E-cad (Cell Signaling, #3195S, 1/250), goat anti-CtxB (Calbiochem #227040, 1/10), and rabbit anti-ms Albumin (Abcam, ab19196, 1/200). F-actin was detected using Alexa Fluor 488 Phalloidin (Invitrogen A12379, 1/100).

Confocal Microscopy

Stained *Drosophila* tissues, sections of murine ileum, and human cell lines (CACO-2, T84) were examined on Leica SP2 or SP5 scanning confocal microscopes. Specific settings for the various experiments varied, but these settings were identical between compared samples (e.g., Figures S2A–S2D).

Electron Microscopy

CACO-2 cells grown on transwell filters or *Drosophila* intestines were fixed in modified Karnovsky's fixative (2.5% glutaraldehyde and 2% paraformaldehyde in 0.15 M sodium cacodylate buffer [pH 7.4]) for 4 hr, postfixed in 1% osmium tetroxide in 0.15 M cacodylate buffer for 1 hr, and stained en bloc in 2% uranyl acetate for 1 hr. Samples were dehydrated in ethanol, embedded in Durcupan epoxy resin (Sigma-Aldrich), sectioned at 50–60 nm, and picked up on Formvar and carbon-coated copper grids. Sections were stained with 2% uranyl acetate for 5 min and Sato's lead stain for 1 min. Grids were viewed using a Tecnai G2 Spirit BioTWIN transmission electron microscope equipped with an Eagle 4k HS digital camera (FEI, Hilsboro, OR).

SUPPLEMENTAL INFORMATION

Supplemental Information includes seven figures and can be found with this article at http://dx.doi.org/10.1016/j.chom.2013.08.001.

ACKNOWLEDGMENTS

We thank Nathalie Franc for generous access to her confocal microscope and helpful comments on the manuscript; Nissi Varki and Liwen Deng for help with preparing and analyzing sections of murine ileal loops; Dr. Marilyn Farquhar for use of the electron microscopy facility; Ying Jones for EM sample preparation; Bill McGinnis, Steve Wasserman, Emily Troemel, Karla Satchell, and members

of the Bier and Nizet labs for helpful discussions; and Allan Fanning and Yang Hong for kindly providing, respectively, the UAS-Pyd-GFP and DECad-tom fly stocks. B.A. is a postdoctoral fellow in the UCSD/SDSU IRACDA Program (GM06852). This study was supported by National Institutes of Health (NIH) R01 grants AI070654 (E.B.) and AI057153 (V.N.).

Received: July 27, 2012
Revised: June 21, 2013
Accepted: July 25, 2013
Published: September 11, 2013

REFERENCES

Apidianakis, Y., and Rahme, L.G. (2011). Drosophila melanogaster as a model for human intestinal infection and pathology. Dis. Model. Mech. *4*, 21–30.

Barrett, K.E. (2006). Water and electrolyte absorption and secretion. In Gastrointestinal Physiology, Chapter 5, J. Malley and C. Naglieri, eds. (New York: McGraw-Hill), pp. 59–100.

Blow, N.S., Salomon, R.N., Garrity, K., Reveillaud, I., Kopin, A., Jackson, F.R., and Watnick, P.I. (2005). *Vibrio cholerae* infection of *Drosophila melanogaster* mimics the human disease cholera. PLoS Pathog. *1*, e8, http://dx.doi.org/10.1371/journal.ppat.0010008.

Boucher, M.J., Laprise, P., and Rivard, N. (2005). Cyclic AMP-dependent protein kinase A negatively modulates adherens junction integrity and differentiation of intestinal epithelial cells. J. Cell. Physiol. *202*, 178–190.

Brand, A.H., and Perrimon, N. (1993). Targeted gene expression as a means of altering cell fates and generating dominant phenotypes. Development *118*, 401–415.

Cheng, S.H., Rich, D.P., Marshall, J., Gregory, R.J., Welsh, M.J., and Smith, A.E. (1991). Phosphorylation of the R domain by cAMP-dependent protein kinase regulates the CFTR chloride channel. Cell *66*, 1027–1036.

Cook, O., Biehs, B., and Bier, E. (2004). *brinker* and *optomotor-blind* act coordinately to initiate development of the L5 wing vein primordium in *Drosophila*. Development *131*, 2113–2124.

Craig, J.P. (1965). A permeability factor (toxin) found in cholera stools and culture filtrates and its neutralization by convalescent cholera sera. Nature *207*, 614–616.

Dahan, S., Rabinowitz, K.M., Martin, A.P., Berin, M.C., Unkeless, J.C., and Mayer, L. (2011). Notch-1 signaling regulates intestinal epithelial barrier function through interaction with CD4(+) T-cells, in mice and humans. Gastroenterology *140*, 550–559.

De, S.N., and Chatterje, D.N. (1953). An experimental study of the mechanism of action of Vibriod cholerae on the intestinal mucous membrane. J. Pathol. Bacteriol. *66*, 559–562.

De Haan, L., and Hirst, T.R. (2004). Cholera toxin: a paradigm for multi-functional engagement of cellular mechanisms (Review). Mol. Membr. Biol. *21*, 77–92.

Ebrahimi, C.M., Sheen, T.R., Renken, C.W., Gottlieb, R.A., and Doran, K.S. (2011). Contribution of lethal toxin and edema toxin to the pathogenesis of anthrax meningitis. Infect. Immun. *79*, 2510–2518.

Fortini, M.E. (2009). Notch signaling: the core pathway and its posttranslational regulation. Dev. Cell *16*, 633–647.

Frömter, E., and Diamond, J. (1972). Route of passive ion permeation in epithelia. Nat. New Biol. *235*, 9–13.

Gabriel, S.E., Brigman, K.N., Koller, B.H., Boucher, R.C., and Stutts, M.J. (1994). Cystic fibrosis heterozygote resistance to cholera toxin in the cystic fibrosis mouse model. Science *266*, 107–109.

Goldenring, J.R., Smith, J., Vaughan, H.D., Cameron, P., Hawkins, W., and Navarre, J. (1996). Rab11 is an apically located small GTP-binding protein in epithelial tissues. Am. J. Physiol. *270*, G515–G525.

Guichard, A., McGillivray, S.M., Cruz-Moreno, B., van Sorge, N.M., Nizet, V., and Bier, E. (2010). Anthrax toxins cooperatively inhibit endocytic recycling by the Rab11/Sec15 exocyst. Nature *467*, 854–858.

Hazelett, C.C., Sheff, D., and Yeaman, C. (2011). RalA and RalB differentially regulate development of epithelial tight junctions. Mol. Biol. Cell *22*, 4787–4800.

Heider, M.R., and Munson, M. (2012). Exorcising the exocyst complex. Traffic *13*, 898–907.

Jafar-Nejad, H., Andrews, H.K., Acar, M., Bayat, V., Wirtz-Peitz, F., Mehta, S.Q., Knoblich, J.A., and Bellen, H.J. (2005). Sec15, a component of the exocyst, promotes notch signaling during the asymmetric division of *Drosophila* sensory organ precursors. Dev. Cell *9*, 351–363.

Jakab, R.L., Collaco, A.M., and Ameen, N.A. (2011). Physiological relevance of cell-specific distribution patterns of CFTR, NKCC1, NBCe1, and NHE3 along the crypt-villus axis in the intestine. Am. J. Physiol. Gastrointest. Liver Physiol. *300*, G82–G98.

Katanayeva, N., Kopein, D., Portmann, R., Hess, D., and Katanaev, V.L. (2010). Competing activities of heterotrimeric G proteins in Drosophila wing maturation. PLoS ONE *5*, e12331, http://dx.doi.org/10.1371/journal.pone.0012331.

Langevin, J., Morgan, M.J., Sibarita, J.B., Aresta, S., Murthy, M., Schwarz, T., Camonis, J., and Bellaïche, Y. (2005). *Drosophila* exocyst components Sec5, Sec6, and Sec15 regulate DE-Cadherin trafficking from recycling endosomes to the plasma membrane. Dev. Cell *9*, 365–376.

Leppla, S.H. (1982). Anthrax toxin edema factor: a bacterial adenylate cyclase that increases cyclic AMP concentrations of eukaryotic cells. Proc. Natl. Acad. Sci. USA *79*, 3162–3166.

Lundgren, O. (2002). Enteric nerves and diarrhoea. Pharmacol. Toxicol. *90*, 109–120.

Maddugoda, M.P., Stefani, C., Gonzalez-Rodriguez, D., Saarikangas, J., Torrino, S., Janel, S., Munro, P., Doye, A., Prodon, F., Aurrand-Lions, M., et al. (2011). cAMP signaling by anthrax edema toxin induces transendothelial cell tunnels, which are resealed by MIM via Arp2/3-driven actin polymerization. Cell Host Microbe *10*, 464–474.

Magnusson, K.E., Kihlstrom, E., and Sundqvist, T. (1985). Effect of cholera toxin on rat intestinal permeability assessed with fluorescent dextran 3000. FEMS Microbiol. Lett. *29*, 15–18.

Mathan, M.M., Chandy, G., and Mathan, V.I. (1995). Ultrastructural changes in the upper small intestinal mucosa in patients with cholera. Gastroenterology *109*, 422–430.

Morize, P., Christiansen, A.E., Costa, M., Parks, S., and Wieschaus, E. (1998). Hyperactivation of the *folded gastrulation* pathway induces specific cell shape changes. Development *125*, 589–597.

Murthy, M., and Schwarz, T.L. (2004). The exocyst component Sec5 is required for membrane traffic and polarity in the *Drosophila* ovary. Development *131*, 377–388.

Murthy, M., Teodoro, R.O., Miller, T.P., and Schwarz, T.L. (2010). Sec5, a member of the exocyst complex, mediates *Drosophila* embryo cellularization. Development *137*, 2773–2783.

Ohishi, I., and Odagiri, Y. (1984). Histopathological effect of botulinum C2 toxin on mouse intestines. Infect. Immun. *43*, 54–58.

Pappenheimer, J.R., and Reiss, K.Z. (1987). Contribution of solvent drag through intercellular junctions to absorption of nutrients by the small intestine of the rat. J. Membr. Biol. *100*, 123–136.

Picciotto, M.R., Cohn, J.A., Bertuzzi, G., Greengard, P., and Nairn, A.C. (1992). Phosphorylation of the cystic fibrosis transmembrane conductance regulator. J. Biol. Chem. *267*, 12742–12752.

Reefman, E., Kay, J.G., Wood, S.M., Offenhäuser, C., Brown, D.L., Roy, S., Stanley, A.C., Low, P.C., Manderson, A.P., and Stow, J.L. (2010). Cytokine secretion is distinct from secretion of cytotoxic granules in NK cells. J. Immunol. *184*, 4852–4862.

Rera, M., Bahadorani, S., Cho, J., Koehler, C.L., Ulgherait, M., Hur, J.H., Ansari, W.S., Lo, T., Jr., Jones, D.L., and Walker, D.W. (2011). Modulation of longevity and tissue homeostasis by the Drosophila PGC-1 homolog. Cell Metab. *14*, 623–634.

Rosenthal, R., Milatz, S., Krug, S.M., Oelrich, B., Schulzke, J.D., Amasheh, S., Günzel, D., and Fromm, M. (2010). Claudin-2, a component of the tight junction, forms a paracellular water channel. J. Cell Sci. *123*, 1913–1921.

Sack, D.A., Sack, R.B., Nair, G.B., and Siddique, A.K. (2004). Cholera. Lancet *363*, 223–233.

Sasmal, D., Guhathakurta, B., Ghosh, A.N., Pal, C.R., and Datta, A. (1995). Studies on adhesion, haemagglutination and other biological properties of Vibrio cholerae O139. FEMS Immunol. Med. Microbiol. *10*, 199–205.

Silvis, M.R., Bertrand, C.A., Ameen, N., Golin-Bisello, F., Butterworth, M.B., Frizzell, R.A., and Bradbury, N.A. (2009). Rab11b regulates the apical recycling of the cystic fibrosis transmembrane conductance regulator in polarized intestinal epithelial cells. Mol. Biol. Cell *20*, 2337–2350.

Strong, T.V., Boehm, K., and Collins, F.S. (1994). Localization of cystic fibrosis transmembrane conductance regulator mRNA in the human gastrointestinal tract by in situ hybridization. J. Clin. Invest. *93*, 347–354.

Triadafilopoulos, G., Pothoulakis, C., Weiss, R., Giampaolo, C., and Lamont, J.T. (1989). Comparative study of Clostridium difficile toxin A and cholera toxin in rabbit ileum. Gastroenterology *97*, 1186–1192.